

X-RAY ENABLED MOCASSIN: A 3D CODE FOR PHOTOIONIZED MEDIA

BARBARA ERCOLANO

Harvard-Smithsonian Center for Astrophysics, MS-67
 60 Garden Street,
 Cambridge, MA 02138, USA

PETER R. YOUNG

STFC Rutherford Appleton Laboratory,
 Chilton, Didcot,
 Oxfordshire, OX11 0QX, UK

JEREMY J. DRAKE & JOHN C. RAYMOND

Harvard-Smithsonian Center for Astrophysics
 60 Garden Street,
 Cambridge, MA 02138, USA
To be submitted to ApJ

ABSTRACT

We present a new version of the fully 3D photoionization and dust radiative transfer code, MOCASSIN, that uses a Monte Carlo approach for the transfer of radiation. The X-ray enabled MOCASSIN allows a fully geometry independent description of low-density gaseous environments strongly photoionized by a radiation field extending from radio to gamma rays. The code has been thoroughly benchmarked against other established codes routinely used in the literature, using simple plane parallel models designed to test performance under standard conditions. We show the results of our benchmarking exercise and discuss applicability and limitations of the new code, which should be of guidance for future astrophysical studies with MOCASSIN.

Subject headings: radiative transfer — plasmas

1. INTRODUCTION

Photoionized environments characterize a wide range of astrophysical problems involving sources of X-radiation. With the advent of new technology used for instruments on board of (e.g.) *XMM-Newton* and *Chandra*, high resolution spectroscopy of such environments has become a reality. Paerels et al. (2000), for instance, observed the photoionized wind in Cygnus X-3 with *Chandra* High Energy Transmission Grating Spectrometer (HETGS) showing the discrete emission to be excited by recombination in a tenuous X-ray-photoionized medium which is not symmetric with the source of the wind. Other examples include the detection of several recombination emission lines (from Fe XXVI at 1.78 Å to N VI at 29.08 Å), by Jimenez-Garate et al. (2005) in a 50 ks observation of the bright X-ray binary Hercules X-1 with *Chandra* HETGS. We also note the *Chandra* ACIS observations of the deeply eclipsing cataclysmic variable DQ Herculis by Mukai et al. (2003), who were able to pin down the origin of the soft X-rays from this system as being due to scattering of the unseen central X-ray source, probably in an accretion disk wind.

A number of 1D photoionization codes, including G. Ferland's CLOUDY (Ferland et al. 1998) and T. Kallman's XSTAR (Kallman & McCray 1980, Kallman & Bautista 2001) continue to represent powerful analytical tools for the analysis of astrophysical spectra from the X-ray to the infrared regime. These codes are designed for diffuse, optically thin media, which may also be irradiated by a non-thermal X-ray continuum, and have been, for instance, applied to the modelling of Narrow

Line Regions (NLRs) of Active Galactic Nuclei (AGNs). Several other codes have been developed which specialize in emission and reflection spectra from optically thick hot photoionized media, irradiated by a non-thermal continuum extending to the hard X-ray region, such as X-ray irradiated accretion disks (e.g. Ross & Fabian, 1993; Nayakshin et al. 2000; Dumont et al. 2000).

To date, these and most other photoionization codes have numerically solved the equations of radiative transfer (RT) under the assumption of spherical symmetry or in plane parallel geometries, whereupon the problem is reduced to a 1D calculation. While very few real X-ray sources are spherically symmetric, this approximation has been driven by the available computing power and the complexity of the multi-dimensional case. Mauche et al. (2004) developed a Monte Carlo code to investigate the radiation transfer of Ly α , He α , and recombination continua photons of H- and He-like C, N, O and Ne produced in the atmosphere of a relativistic black hole accretion disk. This code, however, while accounting for Compton scattering and photoabsorption followed by recombination, does not calculate the ionization state of the plasma. To our knowledge, there are currently no general, self-consistent and publicly available X-ray photoionization and dust RT codes capable of working in 3D. Although the 1D codes mentioned above are powerful tools for the analysis of the pan-chromatic spectra of numerous astrophysical environments, their application is restricted to rather simplified geometries.

The computational demand of realistic 3D simulations has recently come within the reach of low-cost clusters.

Taking advantage of this, the first self-consistent, 3D photoionization and dust RT code was developed for the IR-UV regime using Monte Carlo techniques (Ercolano et al. 2003a, 2005). The code, MOCASSIN (MOnte Carlo SimulationS of Ionized Nebulae) was designed to build realistic models of photoionized environments of arbitrary geometry and density distributions, and can simultaneously treat the dust RT. The code can also treat illumination from multiple point- or arbitrarily extended sources. The fully parallel version of MOCASSIN (documented and publicly available) is well-tested for classical nebulae, according to standard photoionization benchmarks (Péquignot et al., 2001), and has been successfully applied to the modeling of H II regions (e.g. Ercolano, Bastian & Stasińska, 2007) and planetary nebulae (e.g. Ercolano et al. 2003b,c, 2004; Gonçalves et al., 2006; Schwarz & Monteiro, 2006; Wright, Ercolano & Barlow, 2006). We now present a significantly improved version of the MOCASSIN code (version 3.00) which extends to the X-ray regime. In the tradition of previous releases of the MOCASSIN code, the X-ray version will also be made publicly available to the scientific community shortly after publication of this article¹.

In Section 2 we summarize the physical processes and atomic data added/modified in the new implementation and discuss the applicability and limitations of the code in its current form. In Section 3 we compare our code to established 1D codes for benchmark tests, comprising emission line spectra from model NLR and from three thin low-density slab models illuminated by a hard continuum. A brief summary is given in Section 4.

2. THE X-RAY ENABLED MOCASSIN CODE

2.1. Basic philosophy and underlying assumptions

The original MOCASSIN code was developed in order to provide a 3D modelling tool capable of dealing with asymmetric and density and/or chemically inhomogeneous media, as well as, if required, multiple, non-centrally located, point and extended sources of exciting radiation. The code can self-consistently treat the transfer of ionizing and non-ionizing radiation through a medium composed of gas and/or dust. The numerical techniques employed and the physical processes considered by the code are described in detail by Ercolano et al. (2003a, 2005). In brief, MOCASSIN locally simulates the processes of absorption, re-emission and scattering of photons as they diffuse through a gaseous/dusty medium. The radiation field is expressed in terms of energy packets which are the calculation ‘quanta’. The energy packets are created at the illuminating source(s), which may be placed anywhere inside the grid and be of point-like or diffuse nature. Their trajectories through the nebula are computed, as the packets suffer scatterings, absorptions and re-emissions, according to the local gas and dust opacities and emissivities. The packets’ trajectories yield a measure of the local radiation field, from which the local photoionization and recombination rates, as well as the heating and cooling integrals, are determined.

It is worth reminding the reader of the physical assumptions that both the previous and current versions

of the MOCASSIN code rely upon, which also define its applicability and limitations.

- All physical processes affecting the gas are in steady state. This implies that the atomic physics and heating and cooling timescales are short compared to those of gas-motion or to the rate of change of the ionizing field.
- In some cases large optical depths may occur in the core of emission lines of astrophysically abundant ions. As described by Ercolano et al. (2005), resonant scattering is accounted for via an escape probability method. The underlying assumption is that photons in the line centre will be scattered many times in a region close to where they were originally emitted, until they finally escape through the line wings or are destroyed through continuum photo-absorption. While escape probability methods are often used in photoionization models, it is well known that these may lower the accuracy of calculations in high density environments (e.g. Avrett & Loeser, 1988; Dumont et al. 2003). Furthermore, our current scheme assumes a static gas distribution, which would need to be modified to treat winds or accretion disks with very large shear.
- The contribution from recombination is included for H-like, He-like and the lower Fe XXIV lines. Recombination, however, can dominate for several other lines in some extreme cases; in general, this process strengthens the 3s Fe L-lines compared to the 3d (Liedahl et al., 1990). Nevertheless, in the most commonly encountered cases, the contributions from recombination of He-like and H-like species are strongest.
- Very high density environments are problematic and solutions may carry larger uncertainties. Apart from the line transfer issue mentioned above, a higher density limit of $\sim 10^{13} \text{ cm}^{-3}$, at temperatures of $\sim 10^4 \text{ K}$, is imposed by our approximate treatment of three-body recombination and collisional ionization, which become important at higher densities (see also Ferland 2006). However, for highly ionized, hotter gas, e.g. $\sim 10^6 \text{ K}$ gas in the corona of an X-ray binary, the high density limit is increased to $\sim 10^{15} \text{ cm}^{-3}$.
- A treatment for unresolved transition arrays (UTAs), observed in several spectra of AGNs (e.g. Sako et al. 2001), is not currently included in MOCASSIN. Calculations were presented by Behar, Sako and Kahn (2001) for inner shell $n=2-3$ photoexcitation of the 16 iron charge states Fe I through Fe XVI and their data will be included in a future version.

2.2. X-ray extension

2.2.1. Atomic Data

MOCASSIN’s atomic database was updated in order to include the latest data releases. Details of MOCASSIN’s complete database for the original version are given in Appendix A of Ercolano et al. (2003a). Data updates (additions and replacements) implemented for version 3.00 are as follows:

¹ Previous versions are available upon request from BE.

- Free-bound emission for H I, He II and He I uses the data recently calculated by Ercolano & Storey (2006).
- The radiative and dielectronic rates of Badnell et al. (2003), Badnell (2006a,b), Zatsarinny et al. (2003, 2004a,b, 2006), Colgan et al. (2003, 2004), Altun et al. (2004, 2006), Mitnik & Badnell (2004) have been included and are used as default. The data cover all elements up to Zn including sequences up to Na-like electron target, all other species are treated with the previously available data, except for species included in the Nahar (1997,1999) data set, if chosen by the user (see following item).
- The total (radiative and dielectronic) rates of Nahar (1997, 1999) for recombination to all ions of carbon, nitrogen and oxygen and of Nahar (2000) for recombination to Si I, S III, Ar V, Ca VII and Fe XII can now be included, if explicitly chosen. As well as the recombination data set mentioned as the default in the previous item, all data used in previous versions of MOCASSIN are still available for use and compatible with the X-ray version.
- The fits of Verner (1996) to Opacity Project (Seaton et al. 1993) data for the photoionization cross-sections from all shells are used (the previous versions used the same fitting procedures, but only allowed photoionization from the outer valence electron shell).
- The data set for collision strengths, transition probabilities and energy levels has been substantially updated using version 5.2 of the CHIANTI atomic database (Landi et al. 2006, Dere et al., 1997). The updates are described in more detail in Section 2.3. Further updates are planned for the near future when version 6.0 of the database becomes available.
- Recombination lines from hydrogenic species are calculated using fits to the line emissivities of Storey & Hummer (1995). The data includes species up to $Z=8$, and temperatures extending to 10^5 K for $Z \geq 2$. Species with $Z \geq 8$ are calculated by scaling the He II data. The same hydrogenic scaling to He II is also used for species with $2 \leq Z \leq 8$ when the local electron temperatures exceed the highest tabulated temperature of 10^5 K.
- Recombination lines from He-like species are calculated using fits to recombination data that will become publicly available in the next version of CHIANTI database. The available total (direct+cascade) temperature-dependent recombination coefficients to the individual levels are used in the statistical equilibrium matrix that calculates the level populations, such that the final emissivities automatically include contributions from recombination. As well as the radiative-only rates derived from the Mewe et al. (1985) calculations for He-like iron, the dataset also includes more recent data of Porquet & Daubau (2000), which in-

clude dielectronic contributions, when significant, for He-like ions with $Z = 6, 7, 8, 10, 12$ and 14 .

- Recombination contributions to Li-like Fe XXIV transitions are calculated in a similar fashion to He-like contributions (see item above), using the temperature-dependent recombination coefficients of Gu et al. (2003). The data, however, extend only to the 3d level, transitions originating from higher levels (e.g. Fe XXIV 7.99 Å) are calculated via hydrogenic scaling of the coefficients given in Storey & Hummer (1995).
- The ionization rate coefficients of atoms and ions by electron impact now uses the fits presented by Voronov (1997). The collisional ionization and heating effects of the suprathermal secondary electrons following inner-shell photoionization are computed using approximations from Shull & van Steenberg (1985). Ionization by suprathermal secondaries is generally only important for very low ionization fractions.

2.2.2. Inner-shell photoionization

Previous versions of the MOCASSIN code were designed to treat the transfer of low-energy ionizing radiation, typical of H II regions and PNe. In these environments, only ionization from the outer valence electron shell needs to be considered. We have now lifted this limitation by including inner shell photoionization using the Auger yields of Kaastra & Mewe (1993) and the photoionization cross-sections given by Verner et al. (1996). The solution of the ionization balance equations is rendered more complicated by the coupling of non-adjacent states through the emission of multiple electrons by high energy photons. We adopt a similar iteration scheme as that described by Ferland (2006) to solve the resulting ionization balance matrix.

2.2.3. Thomson/Compton scattering

The Compton cross-section is calculated via the Klein-Nishina formula, which simplifies to the Thompson case at non-relativistic energies. Compton heating and cooling contributions are calculated using standard formulae (e.g. Rybicki & Lightman, 1986). Bound Compton ionization and heating from high energy photons ($\gtrsim 2.3$ keV for hydrogen) are also taken into account, using the formalism described by Ferland (2006, Eqn 294).

The great advantage of a 3D Monte Carlo transfer technique is that scattering events can be treated taking into account the real geometry of the object. The reprocessed directions of Compton-scattered packets, for example, are calculated stochastically using probability density functions based on the redistribution functions obtained from the Klein-Nishina formulae. This is of particular interest for the calculation of fluorescence spectra, as described in Drake, Ercolano & Swartz (2007), Drake & Ercolano (2007a) and Drake & Ercolano (2007b), but it can in principle be applied to any line or continuum energy packet.

2.3. Energy levels, collision strengths and radiative decay rates

Energy levels, collision strengths and radiative decay rates have been updated with data from version 5.2 of the CHIANTI atomic database (Landi et al., 2006; Dere et al., 1997). Since highly excited levels are generally not significantly populated in photoionized plasmas, not all data from CHIANTI were converted into the MOCASSIN format. Thus, for example, while the CHIANTI models for many of the boron-like ions consist of 125 levels, only data for the lowest 10 levels are currently used by MOCASSIN. The number of levels used for each iso-electronic sequence are listed in Table 1. The Maxwellian-averaged collision strengths, Υ , are stored as spline fits in CHIANTI (Dere et al. 1997) which allow Υ to be calculated for any temperature. For MOCASSIN, Υ s are calculated from the CHIANTI spline fits for the temperature range $2.0 \leq \log T \leq 6.4$ at 0.2 dex intervals.

Up until version 4 of CHIANTI all collision data were fitted with a five point spline, following the method of Burgess & Tully (1992). For some transitions, however, a five point spline was not able to accurately fit the entire set of collision strengths and thus it was necessary to omit some of the original data points for the fit. The choice of which data points to omit was influenced by the major application of CHIANTI – the analysis of emission line spectra from *collisionally-ionized* plasmas such as the solar corona – thus care was taken to ensure the fits were accurate in the temperature range where the ion was most abundant. (Tables of these temperature ranges are given in Mazzotta et al. 1998, for example.) Oftentimes this led to the collision strength data at low temperatures being omitted from the fit. With version 4 of CHIANTI (Young et al. 2003) nine point spline fits to the collision strength became available as an option, thus allowing improved fits at low temperatures. As it is the low temperatures that are important for *photoionized* plasmas, the early CHIANTI data-sets have been re-assessed to ensure that the low temperature data points are being accurately reproduced. Poor fits were improved by re-fitting the original data with nine point splines. An example of an improved fit to the O IV ground transition is shown in Fig. 1.

In the process of adapting the CHIANTI data files for MOCASSIN, the existing data within MOCASSIN have been compared with those in CHIANTI. In general, MOCASSIN used the same or older atomic data; in the latter case CHIANTI data simply replaced the MOCASSIN data (after the checks described in the previous paragraph had been performed). In some cases, MOCASSIN made use of better atomic data (either more recent calculations, or data more suited to photoionized plasmas), and so these data were assessed and added to CHIANTI. The comparison between CHIANTI and MOCASSIN also proved valuable for identifying errors in the data files and a number of corrections have been made to CHIANTI. These updates will appear in the next version of that database.

3. BENCHMARK TESTS

The complexity of the calculations involved in large scale photoionization codes, where a number of coupled microphysical processes are at play, imposes the need for careful testing before predictions from such codes may be trusted. In terms of energetics, care should be taken that all ionization and recombination, heating and cooling channels are correctly represented.

The new code presented here has been thoroughly tested and compared, for the 1D case, to the solutions to a number of benchmark models obtained by independent codes routinely used in the literature. The set of benchmarks used was presented by Péquignot et al. (2001) and comprises a plane-parallel simulation for conditions typical of NLRs of AGNs and three low-density thin slab models irradiated by a strong broken power-law continuum radiation field, as described in Table 10 of Péquignot et al. (2001), and reproduced here for convenience (see Table 3). For the NLR model the illuminating spectrum is a power law in energy units with slope 1.3, and the ionization parameter, $U_{13.6} = 0.01$ is defined as $F_{13.6} / (c \times n_H)$, where $F_{13.6}$ is the incident photon flux above 13.6 eV. The ionization parameters of the three X-ray slab models, X0.1, X1.0 and X10.0 are $U_{100} = 0.1$, 1.0 and 10.0, respectively, where the definition of U_{100} is analogous to that of $U_{13.6}$ above.

The plane-parallel geometry assumed by the 1D test, can be mimicked with our 3D code by modelling a thin, elongated cuboidal grid with plane parallel diffuse illumination coming at normal incidence from one of the smaller sides; the energy packets are only allowed to escape from the side opposed to the illuminating side and all other sides act as mirrors (for a discussion of the *mirror* technique see Ercolano et al., 2003b). The main input parameters for the benchmark tests are given in Table 1 of Péquignot et al. (2001) and repeated in our Table 2 for convenience.

We run a number of tests to estimate the random error due to Monte Carlo sampling in order to establish an efficient, yet reliable, combination of cell numbers and energy packets needed to sample them. We adopted grids of 300 depth points and three by three in the short axes, with the number of packets needed to achieve convergence varying from one to eight million. Errors of the order of 0.5 % in computed line strengths are common with this setup, with larger errors (<6%) sometimes obtained for the less abundant ions.

We note that radiative transfer effects are largely unimportant for the lines listed in the X-ray slab models. Furthermore, the models are optically thin to ionizing radiation and electron temperature and density, and ionization structure variations through the slabs are minimal.

Before discussing the benchmark results in detail, we note that many atomic data updates and code developments have occurred in the past seven years (see Ercolano 2005). In particular, the radiative and dielectronic recombination coefficients calculated by Badnell et al. (2003), Badnell (2006a,b), Zatsarinny et al. (2003, 2004a,b, 2006), Colgan et al. (2003, 2004), Altun et al. (2004, 2006), Mitnik & Badnell (2004), covering all elements up to Zn (plus Kr, Mo and Xe), including sequences up to Na-like electron target², represent a significant improvement over earlier sets.

3.1. Narrow Line Region

We have organized the benchmark comparison in a similar fashion to Péquignot et al. (2001); for the NLR model we check that MOCASSIN's prediction of each quantity falls within the range of the values obtained by the

² The data set is publicly available from <http://amdpp.phys.strath.ac.uk/tamoc/DATA/>.

other codes, listed in Table 10 of Péquignot et al. (2001). In those cases where MOCASSIN’s prediction lies outside the range, we compute the *isolation factors*, defined as the ratio of the value given by MOCASSIN to the upper limit of the range, if our value is above the range, or the ratio of the lower limit of the range to the value given by MOCASSIN, if our value is below the range. Table 4 lists line fluxes, temperature and ionized helium fraction as predicted by MOCASSIN (column 4) as well as the minimum and maximum values (columns 2 and 3) predicted by the other codes and given in Table 7 of Péquignot et al (2001). The isolation factors computed for MOCASSIN are given in the last column of our Table 4, where we have added a minus or plus sign to indicate whether our prediction lies below or above the range predicted by the other codes.

In Péquignot et al. (2001) it is stated that isolation factors larger than 1.3 should be considered “indicative of a very significant departure and possible problem”. From Table 4 we find that only six out of 48 quantities predicted carried an isolation factor with absolute value larger than 1.3, with only one of these being larger than 2.0. We judge this to be indicative of a high degree of consistency between the results of MOCASSIN and other codes, especially in the light of the atomic physics updates that have occurred between the year 2001 and today. Furthermore, the temperature and ionization structure of our model is also in good agreement with those calculated by other codes indicating that the differences in some line predictions can probably be ascribed to atomic physics changes.

The largest isolation factors were obtained for sulphur ions. The values in Table 4 show that our predictions for the [S III] lines are generally lower than those predicted by other codes, and we suspect that dielectronic recombination effects may be at play in this case. Rates for third row elements are poorly known. In the case of recombination of S IV into S III the rates calculated by Nahar (2000) are available. These calculations used an ab-initio method to derive total (electron+ion) recombination (Nahar & Pradhan 1994, 1995) which enables the consideration of radiative and dielectronic recombination processes in a unified manner. However not all modelers choose to include the total recombination coefficients due to the uncertainties inherent to the method that relies on theoretical predictions of the resonance positions. Here we have used the data of Colgan et al. (2003), which were not available to the 2001 benchmark modelers. Furthermore, no data was available in 2001 for S III \rightarrow S II dielectronic recombination and estimates were used instead (e.g. Ali et al., 1991). Here we used the data of Colgan et al. (2004). It seems likely that some of the scatter recorded for these lines is indeed due the different atomic data available and assumptions made.

As a final note we should add that the temperature at the inner edge calculated by MOCASSIN is slightly lower than the values obtained by the other codes. This is to be expected since MOCASSIN uses a exact treatment of the radiative transfer, including the diffuse component, while comparison codes approximate the transfer of the diffuse component by either iterating along only one direction or by adopting an “outward-only” approximation, but along several directions. As noticed by Péquignot et al. (2001), the kinetic temperature tends to be lower in the inner-

most layers of models with exact transfer, as the ionizing radiation field there is softer. Figure 2 shows electron temperatures, $T_e[K]$, and densities, $n_e[cm^{-3}]$, calculated with MOCASSIN as a function of column density in the slab.

3.2. X-ray irradiated plane-parallel slabs

The Péquignot et al. (2001) benchmarks constitute the first attempt to assess the accuracy of photoionization codes in the X-ray regime. As well as atomic data issues, already pointed out in the previous section, a further complication for this set of models is posed by the fact that, in general, for the far-UV lines listed, the original benchmarks considered sums of multiplet lines in a rather liberal sense, so that *energetics* were privileged at the expense of accuracy of wavelengths (with the exceptions of some fine-structure optical lines). It is therefore possible that part of the scatter amongst the original benchmark values arose because of the different way multiplets have been handled in different model calculations (Péquignot, priv. comm.). This problem persists and should be kept in mind when looking at the comparisons performed in this article. The original benchmark tests were quite rough and their main aim was to highlight gross discrepancies, particularly in derived temperatures. A new benchmarking exercise has yet to appear for the high-energy regime; however it is still useful for us to check our code against the 2001 benchmarks as major problems in the thermal and ionization balances would be uncovered by such a comparison. Furthermore, we propose that the solutions presented here be taken as an improved set, obtained with up-to-date atomic data.

Models of X-ray slabs are assessed by comparing, for each quantity, MOCASSIN’s prediction with the minimum and maximum limits of the range of values obtained by the other codes and listed in Tables 11-13 of Péquignot et al. (2001).

In Figures 3, 4 and 5 we use red (striped) histograms to illustrate MOCASSIN’s results, while the filled and empty black histograms respectively mark the lower and the higher limit of the range of solutions obtained by the other codes in the original exercise. All line fluxes are in units of $[erg\ s^{-1}]$ for a column density of $10^{16}\ cm^{-2}$, with the emissivities being summed over 4π . In aid of future benchmarking efforts we provide in Table 5 the individual line fluxes in $[erg\ s^{-1}]$ as predicted by this version (3.00) of MOCASSIN.

In spite of all the complications listed above, the agreement of MOCASSIN’s predictions with the benchmarks is reassuring and adds confidence to current and future astrophysical applications of the code. In particular, very good agreement is shown for the relative strengths of lines from far infrared to X-ray wavelengths. Some exceptions are discussed in more detail below.

The agreement between MOCASSIN and the codes in Péquignot et al. (2001) for the benchmark X01 is good, although the electron temperature of the slab, listed in Table 5, carries an isolation factor of 1.14. While this is small and not of concern *per se* it may affect the strengths of some of the emission lines.

Figures 4 and 5 demonstrate a very good agreement between MOCASSIN and the codes in Péquignot et al. (2001) for most of the lines listed in Table 5 for benchmarks X1 and X10. The small discrepancies with some of the H-like

TABLE 1
THE NUMBER OF ENERGY LEVELS USED FOR EACH ISO-ELECTRONIC SEQUENCE WHEN COMPILING THE MOCASSIN ATOMIC DATA FILES.

Iso-electronic Sequence	Number of levels	Iso-electronic Sequence	Number of levels
H	9	Na	3
He	17	Mg	5
Li	15	Al	12
Be	10	Si	27
B	10	P	5
C	15	S	5
N	13	Cl	2
O	9	Ar	—
F	2	K	2
Ne	—	Ca	9
		Sc	19

recombination lines (e.g. He II 303.8 Å and H I 1216 Å in X1 and Ar XVIII 20.20 Å, N VII 24.78 Å, C VI 28.47 Å and 33.74 Å and He II 303.8 Å in X10) are most probably due to different extrapolation techniques of the Storey & Hummer (1995) data to the high temperatures of these models.

4. SUMMARY

We have presented a new version of the fully 3D Monte Carlo photoionization code, MOCASSIN. The code was extended to allow the modelling of plasma irradiated by a hard continuum spanning from radio to gamma rays. The atomic data set of the code was also significantly updated and it is now synchronized with the latest release

of the CHIANTI database. The applicability and limitations of the new code were discussed, and the results of a thorough benchmarking exercise presented.

No major problems were found by the benchmark tests, although some minor differences have been found. We have highlighted a number of significant improvements in the atomic datasets available today compared to those available at the time the original benchmark tables were compiled. We provide here updated values and we emphasize the need of a new benchmarking exercise to be undertaken by the plasma modelling community.

The good performance of the MOCASSIN code in all benchmark tests demonstrates that it is ready for application to real astrophysical problems. The public version of the X-ray enhanced MOCASSIN code is available on request from the author.

ACKNOWLEDGMENTS

We thank Daniel Péquignot for crucial guidance with the benchmark comparisons. We also would like to thank Gary Ferland for helpful discussion on solving the ionization balance matrix for non-adjacent stages. Our thanks are also extended to Pete Storey for help with the hydrogenic data set and dielectronic recombination data. We thank the CHIANTI team for making the new data available to us. Finally, we thank the anonymous referee for constructive comments that helped to significantly improve the quality of this work. JJD was supported by the Chandra X-ray Center NASA contract NAS8-39073 during the course of this research. BE was supported by *Chandra* grants GO6-7008X and GO6-7009X.

REFERENCES

- Ali, B., Blum, R. D., Bumgardner, T. E., Cranmer, S. R., Ferland, G. J., Haefner, R. I., & Tiede, G. P. 1991, *PASP*, 103, 1182
 Altun, Z., Yumak, A., Badnell, N. R., Colgan, J., & Pindzola, M. S. 2004, *A&A*, 420, 775
 Altun, Z., Yumak, A., Badnell, N. R., Loch, S. D., & Pindzola, M. S. 2006, *A&A*, 447, 1165
 Avrett, E. H., & Loeser, R. 1988, *ApJ*, 331, 211
 Badnell, N. R., et al. 2003, *A&A*, 406, 1151
 Badnell, N. R. 2006a, *ApJS*, 167, 334
 Badnell, N. R. 2006b, *A&A*, 447, 389
 Burgess A., & Tully J. A. 1992, *A&A*, 254, 436
 Colgan, J., Pindzola, M. S., Whiteford, A. D., & Badnell, N. R. 2003, *A&A*, 412, 597
 Colgan, J., Pindzola, M. S., & Badnell, N. R. 2004, *A&A*, 417, 1183
 Dere, K. P., Landi, E., Mason, H. E., Monsignori-Fossi, B. F., & Young, P. R. 1997, *A&AS*, 125, 149
 Drake, J. J., Ercolano, B., Swartz, D., 2007, *MNRAS*, in press
 Drake, J. J., Ercolano, B., 2007a, *MNRAS*, in press
 Drake, J. J., Ercolano, B., 2007b, *MNRAS*, submitted
 Dumont, A.-M., Collin, S., Paletou, F., Coupé, S., Godet, O., & Pelat, D. 2003, *A&A*, 407, 13
 Dumont, A.-M., Abrassart, A., & Collin, S. 2000, *A&A*, 357, 823
 Ercolano, B., Barlow, M. J., Storey, P. J., & Liu, X.-W. 2003a, *MNRAS*, 340, 1136
 Ercolano, B., Morisset, C., Barlow, M. J., Storey, P. J., & Liu, X.-W. 2003b, *MNRAS*, 340, 1153
 Ercolano, B., Barlow, M. J., Storey, P. J., Liu, X.-W., Rauch, T., & Werner, K. 2003c, *MNRAS*, 344, 1145
 Ercolano, B., Wesson, R., Zhang, Y., Barlow, M. J., De Marco, O., Rauch, T., & Liu, X.-W. 2004, *MNRAS*, 354, 558
 Ercolano, B. 2005, *Planetary Nebulae as Astronomical Tools*, 804, 35
 Ercolano, B., Barlow, M. J., & Storey, P. J. 2005, *MNRAS*, 362, 1038
 Ercolano, B., Bastian, N., & Stasinska, G. 2007, *MNRAS*, in press, arXiv:0705.2726

TABLE 2
INPUT PARAMETERS FOR BENCHMARK MODELS.^a

Model:	NLR	X _{0.1} ^{thin}	X ₁ ^{thin}	X ₁₀ ^{thin}
Ionizing Spectrum	PL1	BPL	BPL	BPL
n_H [cm ⁻³]	10 ⁴	10 ⁵	10 ⁵	10 ⁵
$N(H)^{out}$ [cm ⁻²]	10 ²²	10 ¹⁶	10 ¹⁶	10 ¹⁶
$U_{13.6 eV}$	0.01	—	—	—
$U_{100 eV}$	—	0.1	1	10
He/H	0.1	0.1	0.1	0.1
C/H × 10 ⁵	30.0	37.0	37.0	37.0
N/H × 10 ⁵	10.0	11.0	11.0	11.0
O/H × 10 ⁵	80.0	80.0	80.0	80.0
Ne/H × 10 ⁵	10.0	11.0	11.0	11.0
Mg/H × 10 ⁵	3.0	3.7	3.7	3.7
Si/H × 10 ⁵	3.0	3.5	3.5	3.5
S/H × 10 ⁵	1.5	1.6	1.6	1.6
Ar/H × 10 ⁵	—	0.37	0.37	0.37
Fe/H × 10 ⁵	—	4.0	4.0	4.0

TABLE 3
BROKEN POWER LAW FOR OPTICALLY THIN X-RAY MODELS.

log $h\nu$ (eV)	-4.8663	-0.8663	1.6108	2.0000	5.0000	7.1337
log F_ν (erg)	1.0	14.5	12.7	10.6	7.6	1.0

- Ferland, G. J., Korista, K. T., Verner, D. A., Ferguson, J. W., Kingdon, J. B., & Verner, E. M. 1998, *PASP*, 110, 761
 Ferland, G. J. 2006, *University of Kentucky Internal Report*, 565 pages
 Gonçalves, D. R., Ercolano, B., Carnero, A., Mampaso, A., & Corradi, R. L. M. 2006, *MNRAS*, 365, 1039

TABLE 4
STANDARD NARROW LINE REGION (NLR). ^a

Quantity	Min	Max	MOCASSIN	isolation
H β erg/s/cm ²	1.09	1.49	1.24	0
H β 4861	1.00	1.00	1.00	0
He I 5876	0.100	0.139	0.111	0
He II 4686	0.226	0.260	0.226	0.
C II]2325+	0.362	0.600	0.438	0
C III 1335	0.09	0.148	—	0
C III]1907+1909	2.33	4.09	3.20	0.
C IV 1549+	3.36	4.90	3.84	0.
[NI]5200+5198	0.034	0.230	0.033	-1.03
[NII]6584+6548	1.19	3.27	0.933	-1.28
[NII]5755	0.018	0.310	0.013	-1.39
[NIII]1749+	0.177	0.265	0.157	-1.12
[NIII]57.3 μ m	0.042	0.050	0.041	-1.03
[NIV]1487+	0.203	0.250	0.343	+1.37
NV1240+	0.106	0.191	0.096	-1.10
[OI]63.1 μ m	0.220	3.10	0.156	-1.43
[OI]6300+6363	1.37	2.17	1.44	0
[OII]3726+3729	1.25	1.85	1.23	-1.02
[OIII]51.8 μ m	0.667	0.858	0.919	+1.07
[OIII]88.3 μ m	0.092	0.112	0.117	+1.04
[OIII]5007+4959	31.2	34.9	39.3	+1.12
[OIII]4363	0.286	0.348	0.273	-1.04
[OIV]25.9 μ m	1.72	2.53	1.948	0
OIV]1403+	0.311	0.510	0.374	0
OV]1218+	0.120	0.201	0.148	0
OVI1034+	0.030	0.059	0.041	0
[NeII]12.8 μ m	0.145	0.832	0.165	0
[NeIII]15.5 μ m	1.38	2.86	1.44	0
[NeIII]3869+68	1.64	2.46	1.92	0
[NeIV]2423+	0.394	0.586	0.387	-1.02
[NeV]3426+3346	0.520	0.670	0.456	-1.14
[NeV]24.2 μ m	0.162	0.450	0.340	0
[NeVI]7.63 μ m	0.226	0.288	0.243	0
MgII 2798+	1.23	2.33	1.77	0.
[MgIV]4.49 μ m	0.092	0.116	0.060	-1.53
[MgV]5.61 μ m	0.100	0.230	0.170	0
[SiII]34.8 μ m	0.728	1.37	0.664	-1.09
[SiII]2335+	0.114	0.257	0.177	0
[SiIII]1892+	0.089	0.312	0.130	0
[SiIV]1397+	0.078	0.121	0.101	0
[SiII]6716+6731	0.750	1.86	1.80	0
[SiII]4069+4076	0.082	0.180	0.222	+1.23
[SiIII]18.7 μ m	0.560	0.968	0.284	-1.97
[SiIII]33.6 μ m	0.302	0.488	0.140	-2.16
[SiIII]9532+9069	1.98	2.32	1.30	-1.54
[SIV]10.5 μ m	0.850	1.74	1.57	0
T_{inner} [K]	16840	17100	16250	-1.04
$\langle T[N_{\text{H}} + N_{\text{e}}] \rangle$ [K]	11970	12920	12480	0
$\langle \text{He}^+/\text{He} \rangle / \langle \text{H}^+/\text{H} \rangle$	0.729	0.766	0.736	0

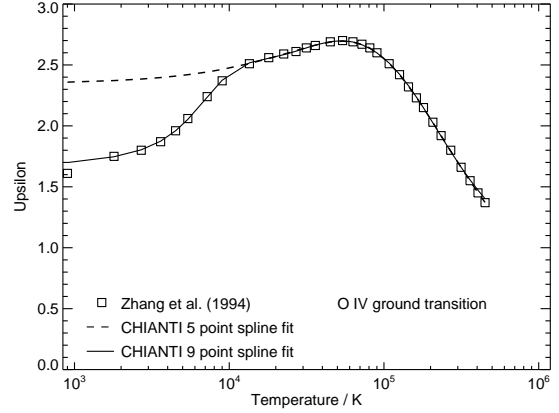


FIG. 1.— Plot demonstrating the difference between five and nine point spline fits for the O IV $^2P_{1/2} - ^2P_{3/2}$ ground transition. The original collision strength data are from Zhang et al. (1994). The five point spline fit was optimized to the temperatures relevant to an electron ionized plasma ($\sim 10^5$ K) and it fails to reproduce the low-temperature region. The nine point spline gives a good fit to the low temperature data points needed for photoionized plasmas.

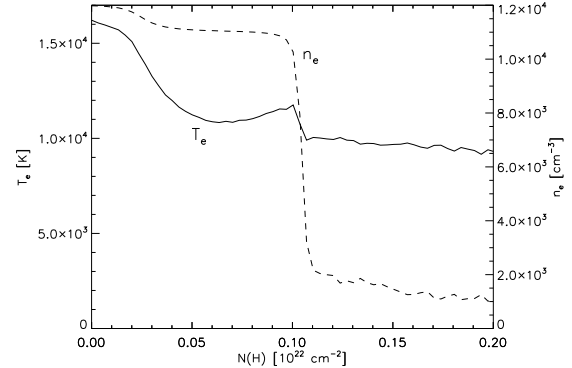


FIG. 2.— NLR benchmark; electron temperature, T_e [K], and density, n_e [cm⁻³], as a function of hydrogen column density, N_{H} [cm⁻²], through the slab.

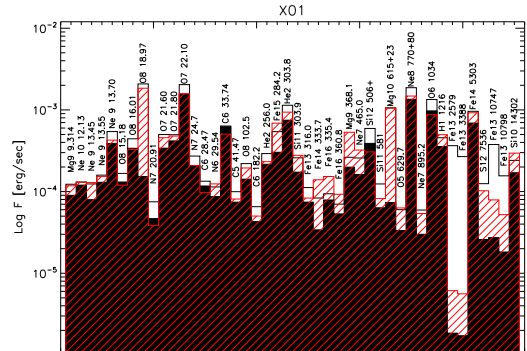


FIG. 3.— X-ray slab; $U_{\text{X}}=0.1$ (X01). The red, striped histograms illustrate MOCASSIN's results, while the filled and empty histograms represent the lower and higher limits of the range of predictions obtained by the codes in Péquignot et al. (2001) .

Gu, M. F. 2003, ApJ, 582, 1241
Kaastra, J. S., & Mewe, R. 1993, A&AS, 97, 443
Kallman, T., & McCray, R. 1980, ApJ, 242, 615
Kallman, T., & Bautista, M. 2001, ApJ, 133, 221
Landi, E., Del Zanna, G., Young, P. R., Dere, K. P., Mason, H. E., & Landini, M. 2006, ApJS, 162, 261
Liedahl, D. A., Kahn, S. M., Osterheld, A. L., & Goldstein, W. H. 1990, ApJ, 350, L37
Mauche, C. W., Liedahl, D. A., Mathiesen, B. F., Jimenez-Garate, M. A., & Raymond, J. C. 2004, ApJ, 606, 168
Mazzotta, P., Mazzitelli, G., Colafrancesco, S., & Vittorio, N. 1998, A&AS, 133, 403
Mewe, R., Gronenschild, E. H. B. M., & van den Oord, G. H. J. 1985, A&AS, 62, 197
Mitnik, D. M., & Badnell, N. R. 2004, A&A, 425, 1153
Mukai, K., Still, M., & Ringwald, F. A. 2003, ApJ, 594, 428
Nahar, S. N., & Pradhan, A. K. 1994, Phys. Rev. A, 49, 1816
Nahar, S. N., & Pradhan, A. K. 1995, ApJ, 447, 966
Nahar, S. N., & Pradhan, A. K. 1997, ApJS, 111, 339
Nahar, S. N. 1999, ApJS, 120, 131
Nahar, S. N. 2000, ApJS, 126, 537
Nayakshin, S., Kazanas, D., & Kallman, T. R. 2000, ApJ, 537, 833

Paerels, F., Cottam, J., Sako, M., Liedahl, D. A., Brinkman, A. C., van der Meer, R. L. J., Kaastra, J. S., & Predehl, P. 2000, ApJ, 533, L135
Péquignot, D., et al. 2001, Spectroscopic Challenges of Photoionized Plasmas, 247, 533
Porquet, D., & Dubau, J. 2000, A&AS, 143, 495

TABLE 5
X-RAY IRRADIATED SLABS. EMISSION LINE FLUXES PREDICTED BY MOCASSIN, GIVEN IN UNITS OF $[erg/s]$.

X01			X1			X10		
Ion	λ [Å]	Flux	Ion	λ [Å]	Flux	Ion	λ [Å]	Flux
Mg9	9.314	1.17E-04	Si16	4.792	7.05E-05	Fe26	1.392	1.98E-05
Ne10	12.13	1.30E-04	Si15	5.101	1.40E-04	Fe26	1.425	4.06E-05
Ne9	13.45	1.29E-04	Si14	6.182	2.30E-04	Fe26	1.503	1.11E-04
Ne9	13.55	1.53E-04	Si13	6.648	7.32E-05	Fe25	1.573	7.75E-05
Ne9	13.70	4.27E-04	Si13	6.688	1.08E-04	Fe26	1.780	6.23E-04
O8	15.18	1.19E-04	Si13	6.740	2.31E-04	Fe25	1.851	5.72E-04
O8	16.01	3.27E-04	Mg12	7.106	4.91E-05	Fe25	1.859	7.81E-04
O8	18.97	1.84E-03	Mg12	8.421	2.38E-04	Fe25	1.868	1.29E-03
N7	20.91	3.86E-05	Mg11	9.314	8.98E-05	Ar18	3.151	1.79E-05
O7	21.60	4.57E-04	Ne10	10.24	9.04E-05	Ar18	3.731	8.75E-05
O7	21.80	4.78E-04	Ne10	12.13	4.14E-04	Si16	3.991	5.76E-05
O7	22.10	1.58E-03	Ne9	13.70	5.61E-05	Ar17	3.994	2.23E-05
N7	24.78	2.07E-04	O8	15.18	1.15E-04	Si16	4.729	2.79E-04
C6	28.47	9.70E-05	O8	16.01	2.94E-04	Si14	4.947	3.17E-05
N6	29.54	1.24E-04	O8	18.97	1.26E-03	Si15	5.101	3.54E-05
C6	33.74	5.04E-04	N7	24.78	9.64E-05	Si14	5.217	8.27E-05
C5	41.47	8.10E-05	C6	33.74	1.68E-04	Si14	6.182	3.78E-04
O8	102.5	1.94E-04	Fe19	101.5	3.23E-05	Si13	6.740	2.34E-05
C6	182.2	5.01E-05	O8	102.5	1.05E-04	Mg12	7.106	4.78E-05
He2	256.0	2.32E-04	Fe19	108.4	1.28E-04	Mg12	8.421	2.10E-04
Fe15	284.2	6.87E-04	Fe22	101+17+36	4.33E-04	Fe26	9.652	6.60E-05
He2	303.8	9.38E-04	Fe20	121.8	3.03E-04	Ne10	10.24	6.57E-05
Si11	303.9	2.77E-04	Fe21	128.0	6.14E-04	Fe25	10.32	7.46E-07
Fe13	316.0	8.33E-05	Fe20	132.8	4.44E-04	Fe24	10.63	1.05E-04
Fe14	333.7	1.39E-04	Fe23	132.8	3.64E-04	Fe24	11.17	3.37E-04
Fe16	335.4	1.52E-04	Fe24	192.0	7.72E-05	Ne10	12.13	2.81E-04
Fe16	360.8	9.27E-05	Fe24	255.1	3.90E-05	O8	16.01	6.57E-05
Mg9	368.1	5.32E-04	He2	303.8	1.64E-04	O8	18.97	2.81E-04
Ne7	465.0	3.22E-04	Ar16	389+	9.34E-05	Ar18	20.20	2.34E-05
Si112	506+	3.05E-04	Si14	418+	1.58E-04	N7	24.78	5.77E-05
Si11	581.0	8.21E-05	Si12	506+	7.30E-05	Si16	25.58	2.64E-05
Mg10	615+23	1.04E-03	Fe20	567.8	4.82E-05	C6	28.47	2.41E-05
O5	629.7	6.30E-05	Fe20	721.4	9.57E-05	Si14	33.42	3.38E-05
Ne8	770+80	1.47E-03	Fe22	845.4	8.52E-05	C6	33.74	9.59E-05
Ne7	895.2	5.39E-05	H1	1216	9.13E-05	Mg12	45.51	1.81E-05
O6	1034	8.74E-04	Fe21	1354	2.14E-04	Ne10	65.56	2.34E-05
H1	1216	4.97E-04	T/10 ⁵ K		6.99	O8	102.5	5.89E-05
Fe13	2579	6.12E-06				Fe23	132.8	1.42E-04
Fe13	3388	5.60E-06				Fe24	192.0	3.09E-04
Fe14	5303	9.21E-04				Fe24	255.1	1.38E-04
Si12	7536	1.02E-04				He2	303.8	7.97E-05
Fe13	10747	7.91E-05				T/10 ⁶ K		1.44
Fe13	10798	5.22E-05						
Si10	14302	2.95E-04						
T/10 ⁴ K		12.2						

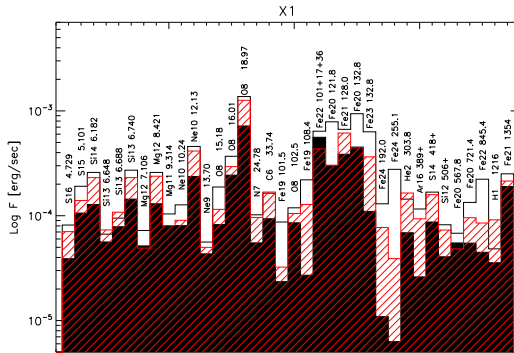


FIG. 4.— X-ray slab; $U_X=1$ (X1). The red, striped histograms illustrate MOCASSIN's results, while the filled and empty histograms represent the lower and higher limits of the range of predictions obtained by the codes in Péquignot et al. (2001).

Rybicki, G. B., & Lightman, A. P. 1986, Radiative Processes in Astrophysics, by George B. Rybicki, Alan P. Lightman, pp. 400. ISBN 0-471-82759-2. Wiley-VCH, June 1986.,
Ross, R. R., & Fabian, A. C. 1993, MNRAS, 261, 74

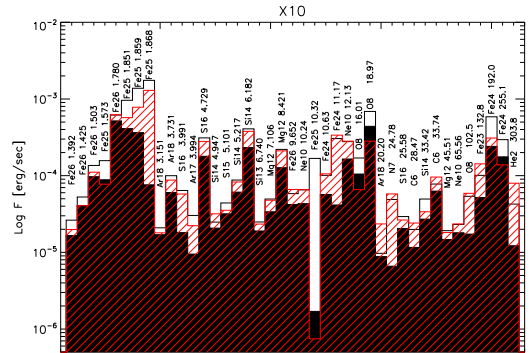


FIG. 5.— X-ray slab; $U_X=10$ (X10). The red, striped histograms illustrate MOCASSIN's results, while the filled and empty histograms represent the lower and higher limits of the range of predictions obtained by the codes in Péquignot et al. (2001).

Schwarz, H. E., & Monteiro, H. 2006, ApJ, 648, 430
Seaton, M. J., Yan, Y., Mihalas, D., & Pradhan, A. K. 1994, MNRAS, 266, 805
Shull, J. M., & van Steenberg, M. 1985, ApJ, 298, 268

- Storey, P. J., & Hummer, D. G. 1995, MNRAS, 272, 41
- Verner, D. A., Ferland, G. J., Korista, K. T., & Yakovlev, D. G. 1996, ApJ, 465, 487
- Voronov, G. S. 1997, Atomic Data and Nuclear Data Tables, 65, 1
- Wright, N., Ercolano, B., & Barlow, M. J. 2006, Planetary Nebulae in our Galaxy and Beyond, 234, 545
- Young, P. R., Del Zanna, G., Landi, E., et al. 2003, ApJS, 144, 135
- Zatsarinny, O., Gorczyca, T. W., Korista, K. T., Badnell, N. R., & Savin, D. W. 2003, A&A, 412, 587
- Zatsarinny, O., Gorczyca, T. W., Korista, K., Badnell, N. R., & Savin, D. W. 2004a, A&A, 426, 699
- Zatsarinny, O., Gorczyca, T. W., Korista, K. T., Badnell, N. R., & Savin, D. W. 2004b, A&A, 417, 1173
- Zatsarinny, O., Gorczyca, T. W., Fu, J., Korista, K. T., Badnell, N. R., & Savin, D. W. 2006, A&A, 447, 379
- Zhang, H. L., Graziani, M., & Pradhan, A. K., 1994, A&A, 283, 319